Void fraction in a co-current two-phase flow through a prototypical PWR spent fuel assembly

Guillaume Brillant, Jimmy Martin

Void fraction in a co-current two-phase flow through a prototypical PWR spent fuel assembly

G. Brillant*, J. Martin

[a]*IRSN, PSN-RES, CEN Cadarache, BP3, Saint Paul lez Durance Cedex, 13115, , France*

Abstract

The Fukushima accident has led in the last decade to numerous studies on the Spent Fuel Pools (SFP) accident phenomenology. In this context, the IRSN has launched an experimental project named DENOPI with the aim to study the behavior of spent fuel pools under loss of cooling and loss of coolant conditions. Within this project, the MEDEA facility is intended to study the thermal-hydraulics of a fully covered or uncovered spent fuel bundle. It consists in a hydraulic loop connected to an experimental test section in which a simulated one meter high PWR spent fuel bundle is located. The MEDEA-overflow experiments, presented in this study, consist in an adiabatic air/water flows in a fully covered unheated bundle. The pressure is measured all along the fuel bundle using several pressure transducers and the void fraction evolution is estimated and analyzed. Two different flow regimes are put in evidence in the MEDEA-overflow test series. Indeed, at low gas superficial velocities, a bubbly flow set up within the bundle whereas a transition to slug flow was obtained at larger ones. Finally, the results of several drift flux models are analyzed and compared to the experimental measurements.

Keywords:
loss-of-cooling/coolant accident, spent fuel pool, two phase flow

*Corresponding author
Email address: guillaume.brillant@irsn.fr (G. Brillant)

1. Introduction

Since the Fukushima-Daiichi accident, much attention has been paid to the vulnerability of Spent Fuel Pools (SFP) [1, 2] and several kinds of actions have been launched in order to understand and reduce the risk and consequences of potential accidents on SFP[3–7]. For instance, a working group set up at OECD/NEA issued a status report on SFP Loss-of-Cooling and Loss-of-Coolant Accident (SFP-LOCA), that aims at providing a summary of the status of SFP accident and mitigation strategies, a brief review of the state of the art of the simulation tools potentialities for SFP-LOCA assessment and a proposal for some additional research actions [8]. Furthermore, a European NUGENIA project named Air-SFP was performed in 2015-2016, in order to assess the uncertainties of Severe Accident (SA) codes in dealing with SFP-LOCA and to identify needs of modeling improvement [9]. Recently, a Phenomena Identification Ranking Table (PIRT) activity related to SFP-LOCA was carried out at OECD/NEA [10]. From these activities, it appears that the validation database of most computer codes currently used for SFP deterministic safety analysis (system codes developed on the basis of in-reactor incidental or accidental conditions) needs to be extended to SFP configurations. Indeed, the thermal-hydraulics of a SFP is mainly based on natural convection flows (gaseous, liquid or two-phase flows), developed at atmospheric pressure with a relatively low heat load, compared to in-reactor conditions. These current codes haven't been primarily developed for natural convection flows and their applicability to SFP has to be improved.

To increase the knowledge and understanding of the SFP accident phenomenology, the DENOPI project [11–13] has been launched by the IRSN (the French Technical Safety Organization) in collaboration with several research laboratories with the aim of studying the behavior of spent fuel pools under Loss-of-Cooling and Loss-of-Coolant Accidents (SFP-LOCA). The DENOPI project is a research program including both experimental and modeling activities. Its purpose is to provide code developers with an experimental database, made up of SFP integral and separate effect tests, for code improvement and validation. The project is divided into three axes, each corresponding to a specific spatial scale involved in a SFP-LOCA. The first axis is related to the two-phase natural convection flows occurring at the pool scale, prior to the fuel uncovery. The thermal-hydraulics of a typical PWR (Pressurized Water Reactor) fuel bundle prior and after the fuel uncovery is investigated in the second axis. In particular, the efficiency of spray

cooling systems as a mitigation measure is assessed. Finally, the third axis is dedicated to the fuel cladding degradation by steam-air mixture oxidation after fuel uncovery.

The main component of the MEDEA facility, which is part of the second axis of the DENOPI project, is a one meter high unheated rod bundle. This experimental set-up aims at getting new insights on the physical phenomena involved during uncovering and water spraying of a fuel bundle stored in a spent fuel pool. Two steps were identified for the MEDEA program. The first one is focused on air/water experiments, and the second one on steam/water experiments. The air/water experiments are of two kinds: the study of flooding in case of water spraying on a completely uncovered bundle (MEDEA-flooding tests) and the study of the void distribution along a fully covered assembly in an air/water co-current flow (MEDEA-overflow tests). The results of the MEDEA-overflow tests are presented in this article. The MEDEA-overflow tests aim at studying pressure and void fraction along a PWR (Power Water Reactor) fuel bundle for a co-current air/water flow at room temperature and atmospheric pressure. These measurements are required for the validation of thermal-hydraulics numerical tools, especially regarding the drift flux models for the low pressure domain of natural flow in a fuel bundle. The aim of this study is to perform a parametric analysis with parameters that can be independently controlled. The influence of the neighbor racks on the physical phenomena inside the central rack is not addressed here but it is part of the objectives of the MIDI facility which is developed within the first axis of the DENOPI project [11, 12]. Besides, this study is carried out under isothermal conditions while the influence of heated rods on the thermal hydraulics will be analysed deeply by means of the forthcoming test loop called ASPIC which is the second test loop build out within the second axis of the DENOPI project.

This article is organized as follows. In section 2, a presentation of the MEDEA device and measurement apparatus is driven. Besides, the test parameters and the experimental protocol are laid out. Then, the results of the test series are stated and analyzed in section 3. Finally, several drift flux model are considered and their results are discussed and compared to experiments in section 4.

2. Experimental set-up

2.1. The overflow configuration of the MEDEA facility

In order to study several time and geometrical scales of the SFP accident in the framework of the DENOPI project, several experimental rigs are planned. The MIDI facility [12, 14] will be devoted to the investigations on large scale flow patterns and onset of boiling in SFP before the dewatering of the fuel bundles. The physical phenomena involved at the assembly scale during a SFP deflooding will be studied in the MEDEA and ASPIC test rigs. Therefore, the IRSN platform THEMA (THErmalhydraulics for Mitigation of Accidents) is growing up with three new significant facilities.

The overflow configuration of the MEDEA facility is composed of a test section with a one meter high rod bundle, an air injection line connected to the bottom of the test section, a water injection line connected to the bottom of the test section, and a water gathering circuit for the overflow liquid (*Cf.* figure 1). The MEDEA assembly consists in a 17x17 rods bundle with a reduced height of 1240 mm for a weight of about 80 kg. The central test section, in which the assembly is inserted, is a square tube with an internal dimension of 225 mm corresponding to a cell of a spent fuel pool rack. The top nozzle, spacer grids, and rods used to build the assembly are representative to a typical PWR rod bundle. The free flow area of the top nozzle is about 205 cm^2. Below the test section with the rod bundle, the lower section aims at injecting the water flow and the air bubbles and obtaining a stationary flow at the bottom of the rod bundle. The length of the lower section is 1416 mm (about 6 hydraulic diameters). Above the test section, the upper head is connected to the gathering water line that collects the overflow.

[Figure 1 about here.]

A flowmeter/valve group is incorporated in the air injection line in order to regulate the air mass flowrate injected in the test section. This flowmeter/valve group is used in automatic mode and the target mass flowrate is stabilized by means of a PID controller. The water injection line is connected to a tank with a capacity of 2000 l. The water is pumped from that tank and flows through a flowmeter/valve group. This group can either be used in manual or automatic mode to set up the water mass flowrate in injection line. The water flows through the central section and the rod bundle. Note

that a bypass line can be partially opened with manual valve to send back part of the water flow directly to the main tank. The water flow above the rod bundle leads to an overflow that is collected and sent back by gravity to the main tank by means of the water gathering line.

2.2. Test parameters and experimental protocol

The experimental protocol of the MEDEA-overflow tests is based on the variation of the air mass flowrate injection while the water mass flowrate and the geometrical configuration are unchanged. The three main parameters of the MEDEA-overflow test series are the water mass flowrate, the air mass flowrate, and the geometrical configuration. Two configurations have been considered: with (configuration C1) and without (configuration C2) the rod bundle inside the central test section. That way, the impact of the rod bundle on the evolution of the pressure and void fraction all along the test section can be directly evaluated. The range of the air mass flowrate is 10 Nl/min to 180 Nl/min (flowrate at 0 °C and 1 atm) and the range of the water mass flowrate is $400\,\mathrm{g\,s^{-1}}$ to $2400\,\mathrm{g\,s^{-1}}$.

The series started with a test at zero air flowrate to determine the default signal of all the pressure transducers. That way, the transducers inherent offset (e.g. due to transducer orientation) as well as the potential dynamic pressure offset can be subtracted from the other tests with positive gas flowrates. Note that the free flow section is not constant along the test section which leads to variations of the water velocity and then of the dynamic pressure. For each test, the signal of the pressure transducers is recorded over at least 10 min at 1 Hz. Hence, stabilized mean and standard deviation values of the pressures can be calculated. The locations of all the pressure transducers are reported in figure 1. The uncertainties of the pressure measurements, considering both the sensor and the supply chain, are 0.05 mbar for the differential pressure transducers $dP_A - dP_G$ and 1.5 mbar for the absolute pressure transducers P_{up} and P_{do}. With such uncertainties, it is worth mentioning that the frictional pressure drop cannot be captured by the transducers. Therefore, the pressure measurements in this study are directly used to evaluate the void fraction inside the test section. As far as the flowrate measurements are concerned, the uncertainties are 1 % for the air flow and 0.1 % for the water flow.

Regarding the absolute pressure measurements, the pressure difference $P_{do} - P_{up}$ can be written as (terms with air density are neglected as well as the dynamic pressure difference between two sensors):

$$dP_Z = P_{do} - P_{up} = (1 - \alpha_Z)\rho_w g h + \rho_w g(H - h) \tag{1}$$

where H is the elevation difference between the two transducers, h the elevation difference between the two connection holes on the central section, and α_Z the mean void fraction along the test section between the two holes where the two transducers P_{up} and P_{do} are connected. Therefore, the void fraction α_Z can be estimated as:

$$\alpha_Z = \frac{\rho_w g H - dP_Z}{\rho_w g h} \tag{2}$$

Concerning the differential pressure measurements, the following expression can be written:

$$dP_i - dP_i^0 = \rho_w g \cdot dh_i - (1 - \alpha_i)\rho_w g \cdot dh_i \quad i = A, \ldots, G \tag{3}$$

with dP_i^0 the offset signal of the differential pressure transducers and dh the elevation difference between the two connections of the dedicated transducer. Therefore, the void fraction can be calculated as:

$$\alpha_i = \frac{dP_i - dP_i^0}{\rho_w g \cdot dh_i} \quad i = A, \ldots, G \tag{4}$$

The void fractions profiles presented hereafter were calculated by means of these expressions.

3. Experimental results

3.1. Pressure evolution at $1200\,\mathrm{g\,s^{-1}}$

In this experimental campaign, the water mass flowrate is set to $1200\,\mathrm{g\,s^{-1}}$ and eleven values of the air mass flowrate are considered in the range 0 Nl/min to 180 Nl/min. As the friction inside the test section evolves with the air mass flowrate, the opening rate of the valve on the water line was adapted on each test to stick to the target value of the water mass flowrate. In doing so, the mean value of the water mass flowrate is kept in the range $1198\,\mathrm{g\,s^{-1}}$ to $1223\,\mathrm{g\,s^{-1}}$ (2 % maximum deviation). It can be noticed that, for all tests, the standard deviation of the water mass flowrate is around $1.5\,\mathrm{g\,s^{-1}}$.

The measurements from the differential pressure transducers, gathered in figure 2, reveal a variation in the range 0 mbar to 6 mbar. The mean value of the pressure difference $P_{do} - P_{up}$ on the test section is given in

figure 3. This pressure difference decreases from 196.0 mbar to 165.9 mbar while the air flowrate rises from 0 Nl/min to 180 Nl/min. Concerning the standard deviation of the pressure signals (*Cf.* figures 4 and 5), it can be noticed that the standard deviation of the differential pressure transducers clearly increases with the air mass flowrate. However, this trend cannot be observed in figure 5 for the absolute pressure measurement on the full height of the section. This can probably be imputed to the higher uncertainty of the absolute pressure transducers. Besides, it can be noted that the standard deviation above the rod bundle (curve A, figure 4) is higher than the standard deviation in the assembly area, revealing a more perturbed flow in this region.

[Figure 2 about here.]

[Figure 3 about here.]

[Figure 4 about here.]

[Figure 5 about here.]

3.2. Void fraction with/without the assembly

The void fractions plotted in figure 6 have been calculated by means of the pressure measurements and equations 2 and 4 for the test series with the rod bundle inserted into the test section. Firstly, the lower values of the void fraction are measured above the rod bundle (transducer A). In fact, these smaller values may be ascribed to the higher section radius above the assembly and to the recirculations observed below the overflow water level. It can be noticed a stabilization at this location of the void fraction around $\sim$7 % for the air mass flowrates higher than 120 Nl/min.

The highest values of the void fraction are measured just below the rod bundle (transducer F) and are due to a plug created by the lower plate below the assembly. Note that this plug grows, as well as the void fraction, as the air mass flowrate rises. Intermediary void fraction are observed all along the rod bundle (transducers B-E) as well as in the lower part of the test section (transducer G). The impact of the grids on the void fraction profiles can be hardly explained. In fact, the transducers B (with a support grid) and D (with a mixing grid) lead to similar void fraction profiles but a different behavior is noted for the transducer E (with a support grid). The void fraction in the lower part of the test section (transducer G) is lower than

the void fraction along the rod bundle. This observation can be imputed to the higher friction in the assembly (due to both rods and grids). The mean void fraction (α_Z) over the full height of the test section measured by the two absolute pressure transducers is among the other void fraction curves measured locally by all the differential pressure transducers.

This test series was repeated without the rod bundle in the central test section in order to give information for the code development and validation. The void fraction measured during the test series without the assembly in the central test section are reported in figure 7 as a function of the air mass flowrate. It can be noticed that the measurements for the transducers B to E are quite clustered due to the absence of the assembly. The void fraction differences between the tests with and without the subassembly in the central section are given in figure 8. The differences of void fraction between with and without bundles tests increase with the air mass flowrate. It is consistent with the fact that the fluid frictions rises with the velocity and hence with the mass flowrates. However, the differences remain below 5 % for the range of value of the air and water mass flowrates. It can be observed that the larger differences are observed for the transducers B to E which corresponds to the area of the rod bundle.

[Figure 6 about here.]

[Figure 7 about here.]

[Figure 8 about here.]

3.3. Repeatability of the test series

The test series at $Q_w = 1200\,\mathrm{g\,s^{-1}}$ with the rod bundle inserted into the test section has been considered to check the repeatability of the measurements. For both test series, the mean and standard deviation values of the water mass flowrate and the air mass flowrate are similar and have a negligible impact on further measurements. A difference from 1 mbar to 5 mbar is noticed for the absolute pressure; which leads to discrepancies up to 3 % of the void fraction (*Cf.* figure 9). The same trend is observed on the differential pressure curves with a difference up to 2 mbar from one test to the other that induces a variation on the void fraction up to 30 % (meaning 7 % void fraction absolute difference). These discrepancies put in light the intrinsic highly unstationary behavior of the hydraulics phenomena involved in the test section.

[Figure 9 about here.]

3.4. Analysis

Two differing behaviors of the two-phase flows have been noticed during the MEDEA-overflow experiments, depending on the investigated geometrical configuration. Those behaviors are discussed below. First of all, with no rod bundle in the test section, the two-phase flows always correspond to a bubbly flow, with no noticeable bubble coalescence along the vertical axis. In this configuration, any increase of the gas superficial velocity leads to a gentle variation of the void fraction in the duct, as seen in figure 11. At low gas superficial velocity, one may note that no clear trend can be observed when the liquid superficial velocity is varied. Visually, the flow exhibits a high level of randomness with bubbles fluctuating in all directions, in spite of their upward net movement.

As far as the rod bundle is inserted in the test section, the two-phase flows exhibit a different behavior. In such a case, a bubbly flow is first visualized for the gas superficial velocities lower than $5\,\mathrm{cm\,s^{-1}}$. When more gas is added to the test section, the flow organizes differently and a cap-bubbly flow is reached, in which big gas pockets can be identified. The latter results from the coalescence of individual bubbles, promoted by the confinement imposed to the flow by the presence of the rod bundle. From that point, some big gas pockets accumulate sometimes below the rod bundle upper tie plate, thereby leading to macro-scale flow recirculations. Those recirculations are evidenced by tiny bubbles flowing downwardly and counter-currently to the main flow direction. As seen in figure 10, an increase of the gas superficial velocity also leads to bigger void fractions. But, contrarily to the case with no bundle, a clear trend is observed here regarding changes in liquid superficial velocities: when more liquid is added to the test section, the void fraction reduces accordingly. Noticeably, for high liquid superficial velocities, this latter trend yields void fractions very close to the ones obtained with no rod bundle. It is assumed that an increasing liquid superficial velocity promotes bubbles dispersal by turbulent mixing within the test section and prevents big gas pockets formation and accumulation below the upper tie plate: qualitative flow observations show that those pockets are hardly visible in the test section at higher liquid superficial velocities.

[Figure 10 about here.]

[Figure 11 about here.]

4. An assessment of available models for the prediction of in-pool PWR bundle void fraction

As discussed in this article, only few experimental studies dedicated to in-pool bundle conditions were performed in the past. Most of them were focused on Boiling Water Reactors (BWR) spent fuel two-phase flows under pool storage conditions [15–17]. Those past experiments showed that the phenomenon involves basically two-length scales and are geometry-dependent. Under SFP boiling conditions, a two-phase flow might hence develop within the fuel bundle both at subchannel and casing scales. The latter triggers with a great effect the two-phase flow patterns, as observed by *Chen et al.* [18]. In some cases, a clear recirculation set up between the inner and outer bundle regions, as observed too in the present study (Section 3.4). A class of models, referred to as *drift-flux*, is particularly relevant when dealing with this kind of configurations and is widely used for predicting void fractions within 1D bundle flows [19]. The drift-flux approach assumes that the two phases, flowing into the system of interest, can be assimilated to an intimate mixture. But, contrary to the so-called *Homogeneous Equilibrium Model* (HEM), a 1D drift-flux model postulates the existence of some known phasic velocity and void fraction profiles within the system [19]. The relationship between those profiles is then modeled by means of correlations developed on the basis of dedicated experiments. The latter contain the knowledge of the main flow characteristics, such as, for instance, the above geometrical effects or the two-phase flow topology (e.g. bubbly or churn flow). Further on, those drift-flux models can either be used as a standalone approach or as a support to the closure of the interfacial friction term of the more sophisticated *Two-Fluid Model* [20]. If many models have been developed in the past for predicting such two-phase bundle flows [21], most of them relate to in-reactor configurations and only a few models are relevant for simulating the low-flow, low-pressure and geometrical features characterizing the conditions of a pool storage [22]. In this section, we compare the standalone prediction of three relevant pool bundle drift-flux models to the experimental data obtained by means of the MEDEA facility. The compared void fraction, later denoted as α_C, corresponds to the values of that very variable, deduced from the differential pressure measurement at position C, i.e. within the central region of the bundle, for avoiding any boundary effect (*Cf.* figure 1). The selected models are those of *Julia et al.* [23], *Kamei et al.* [17] and *Murase et al.* [15], that were all specifically developed for treating BWR in-pool bundle

flows. The interested reader may refer to the recent review [22] which gives an in-depth insight into those models. The obtained results are presented in figure 12.

[Figure 12 about here.]

First, one may observe that those three models yield approximately the same prediction for moderate void fractions, up to 5 %. Then, *Julia et al.* model is clearly diverging from the experimental data, in a somewhat exponential fashion. However, the predictions based on *Murase et al.* and *Kamei et al.* models remain close to each other and almost stand around ±30% of the ideal solution, here represented as a solid line. In average, the relative error between the prediction and the experimental data is of 108%, 22% and 58%, respectively for *Julia et al.*, *Kamei et al.* and *Murase et al.* models.

The higher discrepancies between the estimations using the model of *Julia et al.* and the presented data is not surprising. Indeed, in spite of its description of geometrical effects that may occur during an in-pool bundle flow, the model was developed for a forced convection configuration, i.e. characterized by higher phasic velocities when compared to the present data. Interestingly, *Kamei et al.* and *Murase et al.* models, both developed on the basis of a set of BWR-like bundle experimental data, succeed in predicting the void fractions obtained in the PWR-like bundle configuration of the MEDEA-overflow facility, thereby indicating that the geometrical differences between those layouts and their resulting effects are most likely negligible in first approach. At last, *Kamei et al.* model yields better predictions in the low void fraction range and may hence be preferred for in-pool PWR bundle flow simulations.

5. Conclusion

The understanding of the physical phenomena involved at the fuel assembly scale in a spent fuel pool in case of loss of cooling or loss of coolant accidents has been improved thanks to the DENOPI project. The MEDEA-overflow experiments consist in a co-current air/water flow through a one meter height unheated rod bundle inserted into a SFP rack. No clear impact of the mixing grids and support grids on the void fraction profiles could be evidenced in the present experiments. Besides, two flow regimes were put in light. At low gas superficial velocities, a bubbly flow set up within the bundle whereas a transition to slug flow was observed at larger velocities.

Then, a comparison was made between the experimental void fractions and their prediction based on three drift-flux models of the literature, dedicated to in-pool bundle flows. This work allowed identifying a best-suited model. The latter is the *Kamei et al.* model, which yielded accurate predictions in the void fraction range explored in the present study. In the near future of the DENOPI project, the ASPIC facility, with a heated full height rod bundle, will enable several kinds of experiments and scenarios for SFP accidents at the assembly scale.

Acknowledgements

The DENOPI project is part of the "Investment for the future" program funded by the French Government within the framework of the post-Fukushima surveys identified as major safety issues (contract number ANR 11 - RSNR 006).

References

[1] D. Wang, I. Gauld, G. Yoder, L. Ott, G. Flanagan, M. Francis, E. Popov, J. Carbajo, P. Jain, J. Wagner, J. Gehin, Study of Fukushima Daiichi nuclear power station unit 4 spent-fuel pool, Nucl. Tech. 180 (2) (2012) 205–215.

[2] J. Song, T. Kim, Severe accident issues raised by the Fukushima accident and improvements suggested, Nucl. Eng. Tech. 46 (2) (2014) 207 – 216.

[3] Y. Kaji, Y. Nemoto, T. Nagatake, H. Yoshida, M. Tojo, D. Goto, S. Nishimura, H. Suzuki, M. Yamato, S. Watanabe, Study on loss-of-cooling and loss-of-coolant accidents in spent fuel pool, (1) overview, in: Proc. ICONE-27 conference, no. 1343, Ibaraki, Japan, May 19-24, 2019.

[4] T. Nagatake, M. Shibata, H. Yoshida, Y. Nemoto, Y. Kaji, Study on loss-of-cooling and loss-of-coolant accidents in spent fuel pool (3) thermal-hydraulics experiment by using simulated 4x4 fuel bundle for constructing validation database, in: Proc. ICONE-27 conference, no. 1642, Ibaraki, Japan, May 19-24, 2019.

[5] Y.-S. Chen, Y.-R. Yuann, Accident mitigation for spent fuel storage in the upper pool of a Mark III containment, Ann. Nucl. Energy 91 (2016) 156 – 164.

[6] X. Wu, W. Li, Y. Zhang, W. Tian, G. Su, S. Qiu, Analysis of accidental loss of pool coolant due to leakage in a PWR SFP, Ann. Nucl. Energy 77 (2015) 65–73.

[7] N. Tsukamoto, Study on modeling of spray cooling for spent fuel pool accidents, J. Nucl. Sci. Tech. 56 (11) (2019) 945–952. doi:10.1080/00223131.2019.1626778.

[8] Status report on spent fuel pools under loss-of-cooling and loss-of-coolant accident conditions, Tech. Rep. NEA/OCDE 2015-2, Nuclear Energy Agency (OCDE) (2015).

[9] O. Coindreau, B. Jäckel, F. Rocchi, F. Alcaro, D. Angelova, G. Bandini, Severe accident code-to-code comparison for two accident scenarios in a spent fuel pool, in: The 8th European Review Meeting on Severe Accident Research - ERMSAR, 2017.

[10] PIRT: R&D priorities for loss-of-cooling and loss-of-coolant accidents in spent nuclear fuel pools, Tech. Rep. NEA/OCDE 2017-18, Nuclear Energy Agency (OCDE) (2017).

[11] J. Martin, G. Brillant, C. Duriez, N. Trégourès, C. Marquié, The IRSN DENOPI project: a research program on spent-fuel-pool loss-of-cooling and loss-of-coolant accidents, in: NURETH, Xi'an, China, no. 1, 2017.

[12] J. Martin, Overview of the IRSN DENOPI project on spent fuel pool in loss-of-cooling and loss-of-coolant accident conditions, in: CSARP, Bethesda, Maryland, USA, 2016.

[13] H. Mutelle, I. Tamburini, C. Duriez, S. Tillard, N. Trégourès, A. Toutant, M. Mermoux, V. Peres, H. Buscail, A new research program on accidents in spent fuel pools: the DENOPI project, in: WRFPM, Sensai, Japan, no. 100071, 2014.

[14] N. Trégourès, The DENOPI project: a research program on SFP under loss-of-cooling and loss-of-coolant accident conditions, in: IAEA, IE8M, 2015.

[15] M. Murase, H. Suzuki, T. Matsumoto, M. Naithoh, Countercurrent gas-liquid flow in boiling channels, J. Nucl. Sci. Tech. 23 (1986) 487–502.

[16] T. Ishizuka, S. Morooka, T. Kurosu, T. Aoki, M. Futakuchi, M. Yagi, S. Morooka, A. Hoshide, K. Yoshimura, Void fraction correlation for rod bundle, void fraction correlation based on void data of bwr fuel assembly measured by x-ray ct scanner, J. Japan Atomic Soc. 37 (1995) 133–143.

[17] A. Kamei, S. Hosokawa, A. Tomiyama, I. Kinoshita, Void fraction in a four by four rod bundle under a stagnant condition, in: Proc. NUTHOS-7 conference, Seoul, Korea, 2008.

[18] S.-W. Chen, Y. Liu, T. Hibiki, M. Ishii, Y. Yoshida, I. Kinoshita, M. Murase, K. Mishima, Experimental study of air-water two-phase flow in an 8x8 rod bundle under pool condition for one-dimensional drift-flux analysis, Int. J. Heat and Fluid Flow 33 (2012) 168–181.

[19] M. Ishii, T. Hibiki, Thermo-Fluid Dynamics of Two-Phase Flow, 2nd Edition, Springer, 2011.

[20] T. Lopez, D. Bestion, L. Matteo, Validation of a drift-flux model used in the cathare code for rod bundle geometry at low pressure and low liquid flow conditions, in: Proc. 18th NURETH conference, American Nuclear Society, Portland, Oregon, USA, Aug. 18-22, 2019.

[21] P. Coddington, R. Macian, A study of the performance of void fraction correlations used in the context of drift-flux two-phase flow models, Nucl. Eng. Des. 215 (3) (2002) 199–216. doi:https://doi.org/10.1016/S0029-5493(01)00503-9.
URL https://www.sciencedirect.com/science/article/pii/S0029549301005039

[22] S.-W. Chen, Y. Liu, T. Hibiki, M. Ishii, Y. Yoshida, I. Kinoshita, M. Murase, K. Mishima, One-dimensional drift-flux model for two-phase flow in pool rod bundle systems, Int. J. Multiphase Flow 40 (2012) 166–177.

[23] J. Julia, T. Hibiki, M. Ishii, B.-J. Yun, G.-C. Park, Drift-flux model in a sub-channel of rod bundle geometry, Int. J. Heat and Mass Transfer 52 (2009) 3032–3041.

List of Figures

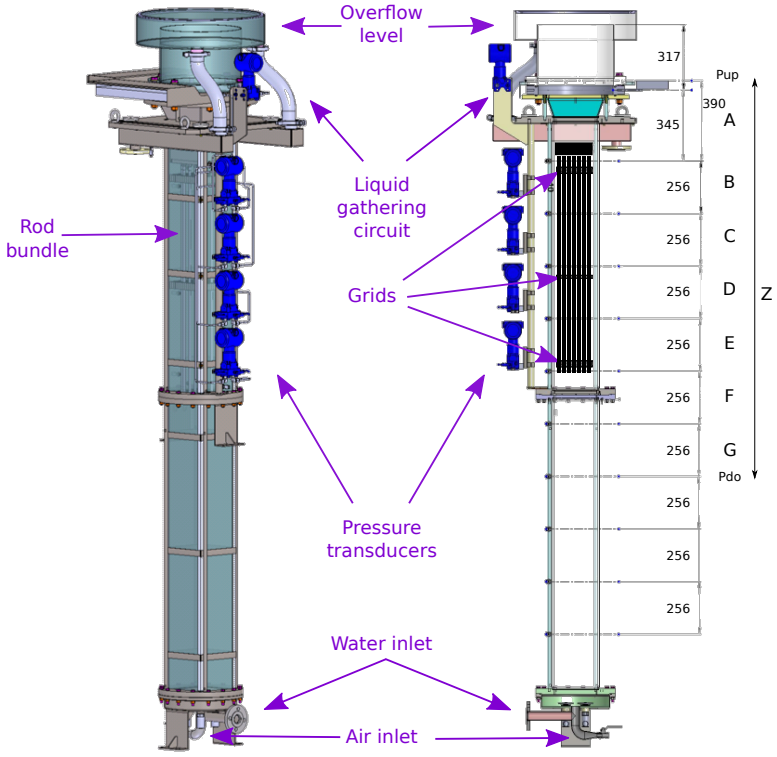

Figure 1: MEDEA-overflow test section with the locations of the pressure measuring holes (A to G).

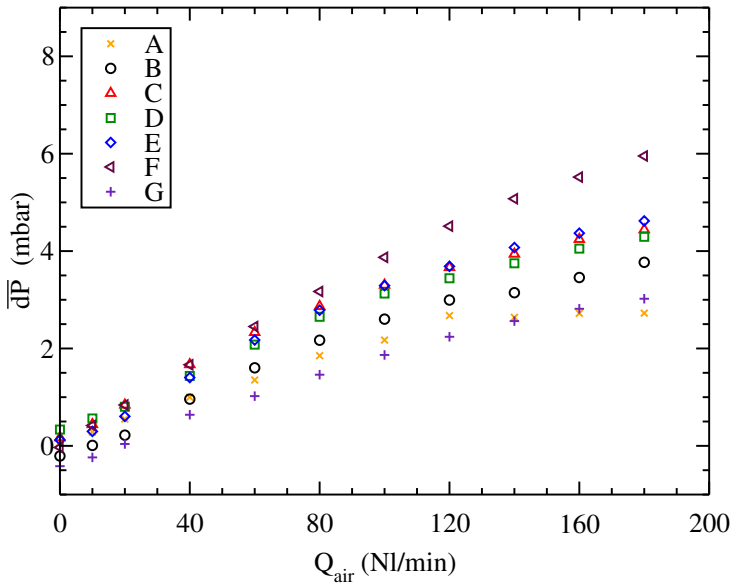

Figure 2: Mean pressure measurements for the tests at a water flowrate of $1200\,\mathrm{g\,s^{-1}}$ from the differential transducers.

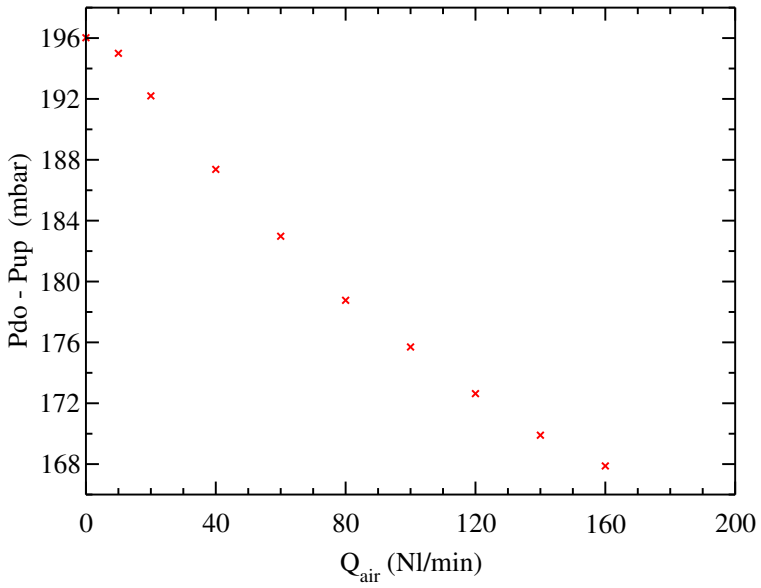

Figure 3: Mean pressure measurements for the tests at a water flowrate of $1200\,\mathrm{g\,s^{-1}}$ from the absolute transducers.

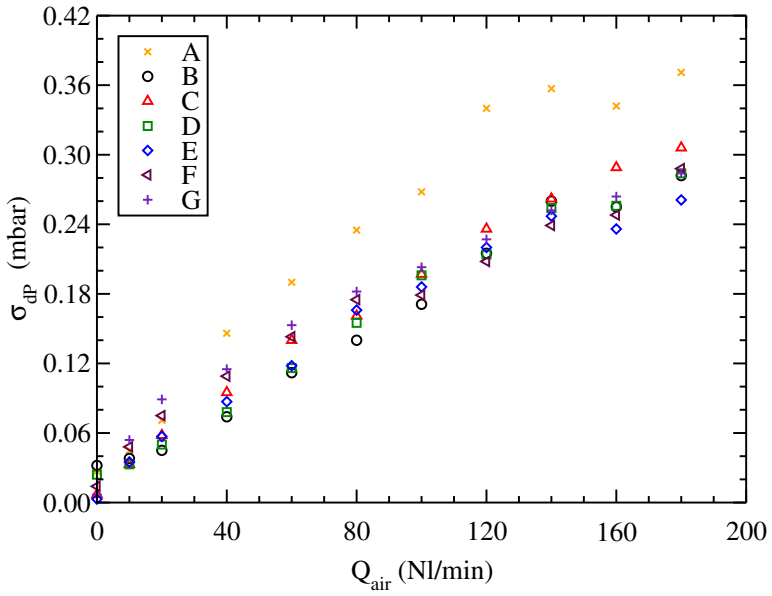

Figure 4: Standard deviation of the pressure measurements for the tests at a water flowrate of $1200\,\mathrm{g\,s^{-1}}$ from the differential transducers.

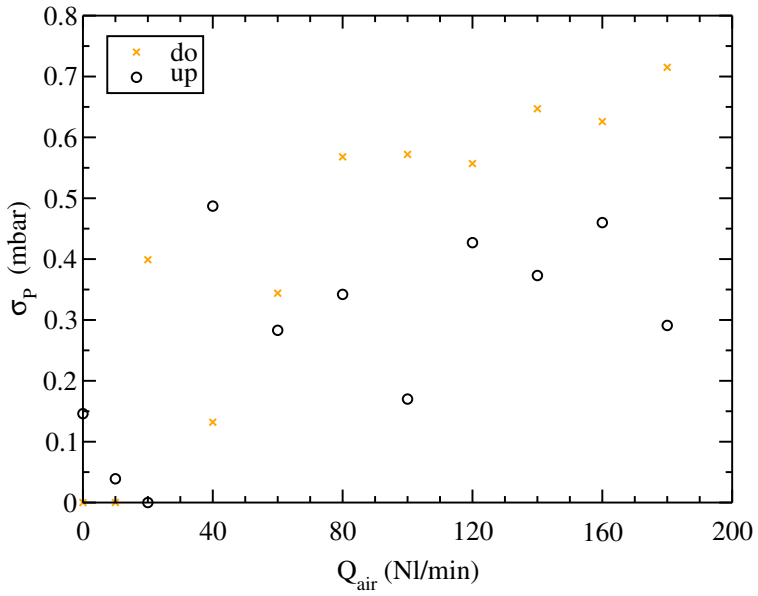

Figure 5: Standard deviation of the pressure measurements for the tests at a water flowrate of $1200\,\mathrm{g\,s^{-1}}$ from the absolute transducers.

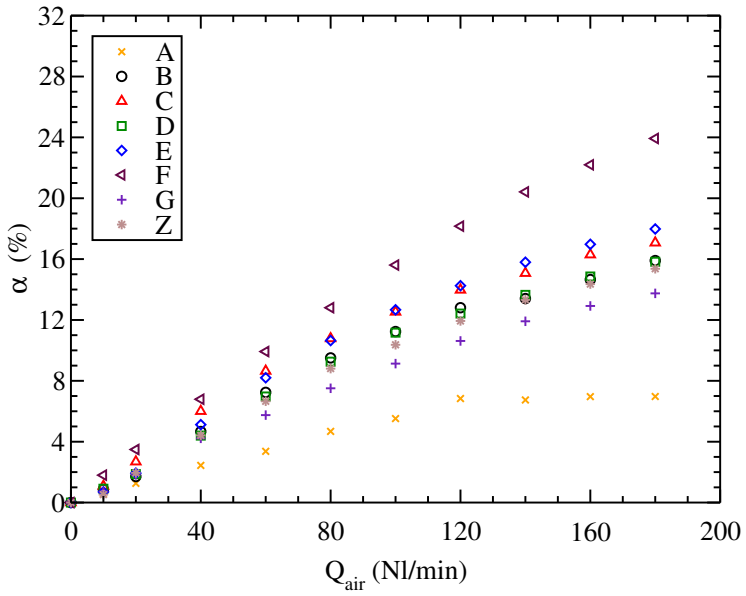

Figure 6: Void fraction for the tests at a water mass flowrate of $1200\,\mathrm{g\,s^{-1}}$ and with the bundle.

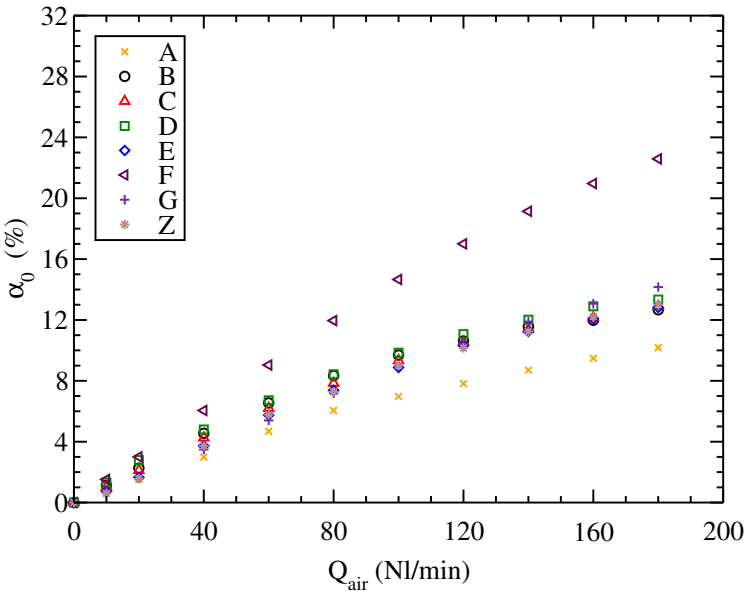

Figure 7: Void fraction for the tests at a water mass flowrate of $1200\,\mathrm{g\,s^{-1}}$ and without the bundle

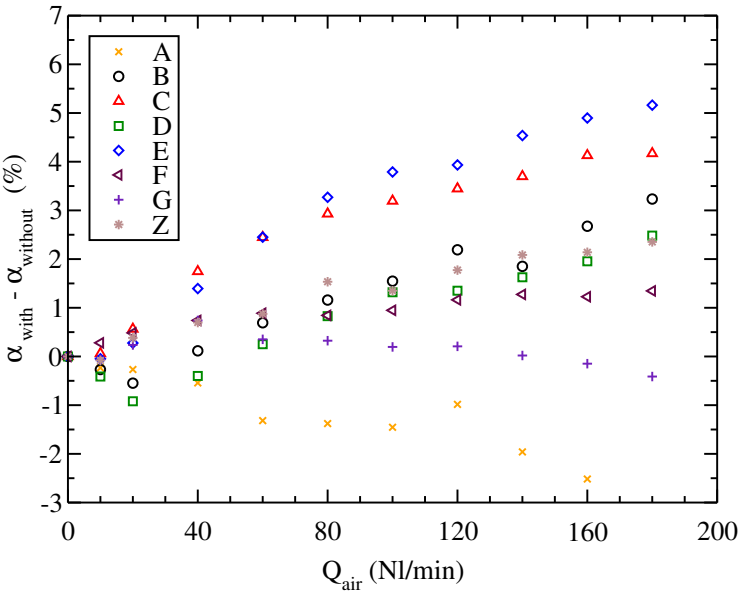

Figure 8: Void fraction difference for the tests with/without assembly at a water flowrate of $1200\,\mathrm{g\,s^{-1}}$.

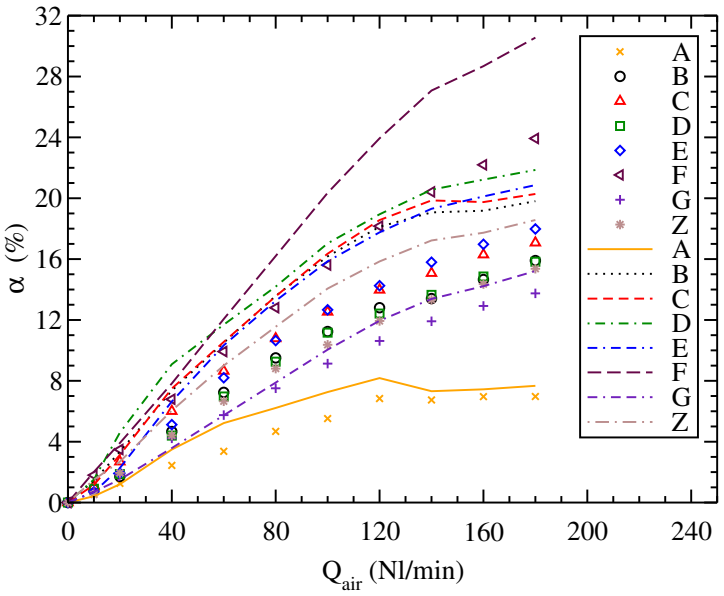

Figure 9: Comparison of the void fraction for the two tests series at a water flowrate of $1200\,\mathrm{g\,s^{-1}}$ (repeatability).

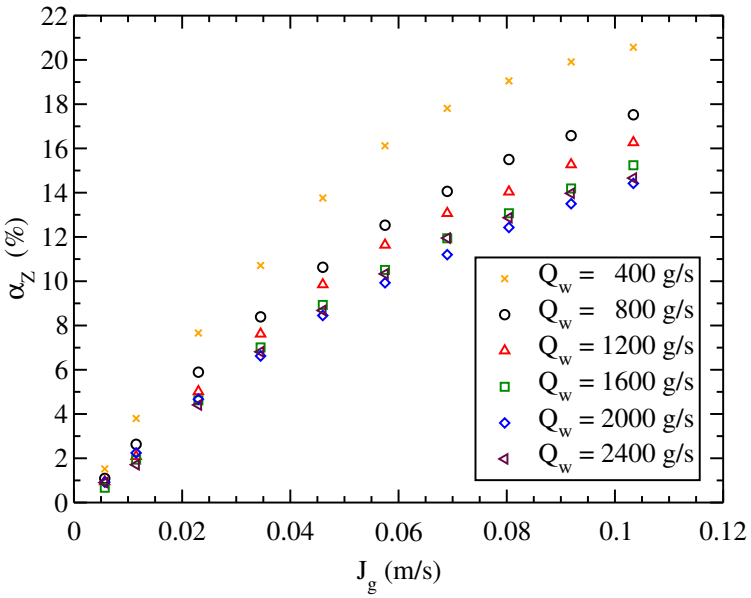

Figure 10: Mean void fraction over vertical direction as a function of the gas superficial velocity (J_g) with bundle

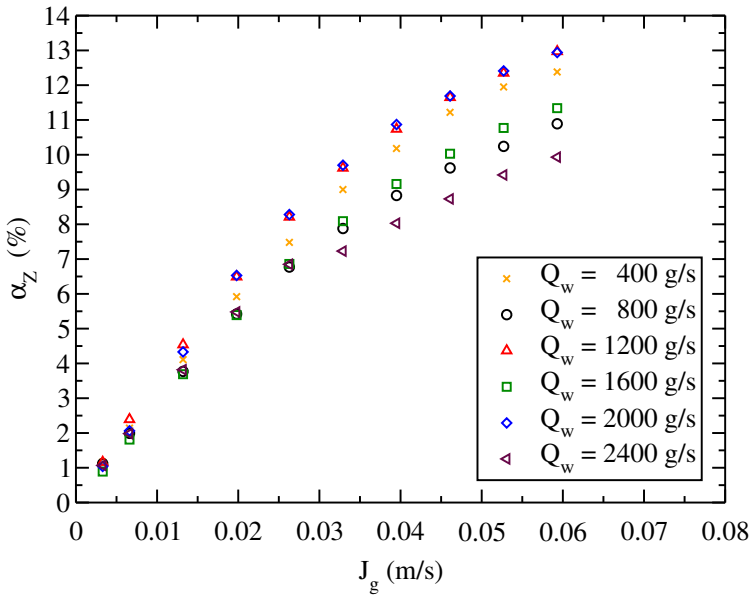

Figure 11: Mean void fraction over vertical direction as a function of the gas superficial velocity (J_g) without bundle

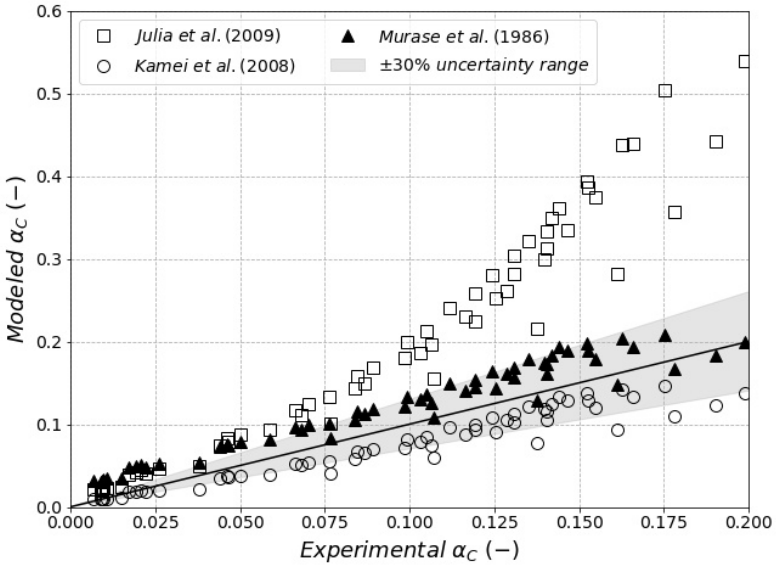

Figure 12: A comparison between the experimental in-bundle void fraction and its prediction based on three relevant drift-flux models.